High Utilization of Composite Magnesium Metal Anodes Enabled by a Magnesiophilic Coating

Yuanjian Li,[a] Gaoliang Yang,[a] Shengnan Sun,[a] Chang Zhang,[b] Carina Yi Jing Lim,[a] Andrew Jun Yao Wong,[a] Wei Ying Lieu,[a] Zdenek Sofer,[c] Man-Fai Ng,[d] Wei Liu,[b] Zhi Wei Seh[a,*]

[a] *Institute of Materials Research and Engineering, Agency for Science, Technology and Research (A*STAR), 2 Fusionopolis Way, Innovis, Singapore 138634, Singapore*

[b] *School of Physical Science and Technology, ShanghaiTech University, Shanghai 201210, China*

[c] *Department of Inorganic Chemistry, University of Chemistry and Technology Prague, Technická 5, 166 28 Prague 6, Czech Republic*

[d] *Institute of High Performance Computing, Agency for Science, Technology and Research (A*STAR), 1 Fusionopolis Way, Connexis, Singapore 138632, Singapore*

Corresponding Authors

*To whom correspondence should be addressed. Email: *sehzw@imre.a-star.edu.sg*

ABSTRACT: Metallic magnesium is a promising high-capacity anode material for energy storage technologies beyond lithium-ion batteries. However, most reported Mg metal anodes are only cyclable under shallow cycling ($\leq$ 1 mAh cm^{-2}) and thus poor Mg utilization (< 3%) conditions, significantly compromising their energy-dense characteristic. Herein, for the first time, composite Mg metal anodes with high capacity utilization of 75% are achieved by coating magnesiophilic gold nanoparticles on copper foils. Benefiting from homogeneous ionic flux and uniform deposition morphology, the Mg-plated Au-Cu electrode exhibits high average Coulombic efficiency of 99.16% over 170 h cycling at 75% Mg utilization. Moreover, the full cell based on Mg-plated Au-Cu anode and Mo_6S_8 cathode achieves superior capacity retention of 80% after 300 cycles at a low negative/positive ratio of 1.33. This work provides a simple yet effective general strategy to enhance Mg utilization and reversibility, which can be extended to other metal anodes as well.

Keywords: Magnesium metal anodes, Magnesiophilic coating, High utilization, High reversibility, Magnesium batteries

The ever-increasing applications in smart electronics and electrification call for high-energy-density electrochemical storage systems beyond the capabilities of state-of-the-art lithium-ion batteries (LIBs).[1-5] Rechargeable magnesium batteries (RMBs) have attracted academic and industrial attention due to metallic magnesium (Mg) offering a high theoretical volumetric capacity of 3833 mAh cm^{-3} (*vs.* 2046 mAh cm^{-3} for metallic

lithium and 818 mAh cm^{-3} for graphite), in addition to its abundant and inexpensive resources.[6-8] However, magnesium metal anodes (MMAs) usually exhibit low Coulombic efficiency (CE) and poor cycling stability during Mg plating/stripping cycles in conventional organic electrolytes.[9-11] Several effective strategies, such as designing electrolyte formulations,[12-15] introducing electrolyte additives,[16-18] and constructing artificial solid electrolyte interphases (SEI),[19-22] have been conducted to improve the reversibility of MMAs. Despite the exciting progress, most reported MMAs are only cyclable under shallow cycling conditions,[23-25] e.g., a typical commercial Mg metal foil (~ 0.1 mm thick) with a large theoretical areal capacity of ~ 38.33 mAh cm^{-2} is usually only charged and discharged to a depth of ≤ 1 mAh cm^{-2}. This poor capacity utilization of MMAs (< 3%) leads to a severely limited actual volumetric capacity (≤ 100 mAh cm^{-3}), much lower than that of commercial graphite and metallic Li anodes in LIBs (Figure 1a), which significantly compromises the energy-dense characteristic of RMBs for practical battery applications.

Considering that the Mg metallic foil as an MMA is present in significant excess (Figure 1b), it is necessary to replace it with a composite magnesium anode, which is usually fabricated by electroplating a small amount of Mg onto a conductive current collector (Figure 1c),[26-28] for higher anode utilization in RMBs. Commercial copper foil is the most extensively used anode current collector in the industry owing to its low price, easy availability, high electronic conductivity, and excellent (electro)chemical stability.[29-31] However, the magnesiophobic surface of Cu foil is adverse to Mg^{2+} desolvation from the stable cation-solvent complex (e.g., $[Mg(solvent)_n]^{2+}$) in

conventional liquid electrolytes, leading to a Mg-ion concentration gradient at the electrolyte/electrode interface (Figure 1d).[16, 28] The Mg^{2+} adsorption and subsequent reduction to Mg on the Cu foil surface prefers to occur at the tips where the ionic flux and coupled electric field distribution are locally aggregated, resulting in inhomogeneous Mg deposits with porous and dendritic morphologies.[32, 33] During the charge-discharge cycles, the noncompact Mg-plated Cu composite anode undergoes drastic volume change, which not only exacerbates the side reaction with liquid electrolytes to generate a thick passivation film,[34, 35] but also continuously consumes active Mg and generates "dead" Mg.[36, 37] All these shortcomings degrade the rechargeability and shorten the lifespan of composite magnesium anodes, even causing safety risks such as short circuits. A recent report observed that modification of metal substrates can suppress Mg dendrite growth,[38] but long-term electrochemical cycling data after modification was not reported, and the effect on Mg deposition dynamics and Mg-ion flux distribution is still unclear. To date, research on current collector engineering for composite Mg anodes is still in its infancy, and their electrochemical performance in RMB remains far from practical application, especially in the case of high Mg metal utilization.

In this work, we developed a modified commercial Cu foil with a magnesiophilic Au nano-coating, to enable a deeply cycled composite Mg anode with unprecedented Mg utilization of 75%. The conformal Au coating, which is ultralight (~ 0.11 mg cm^{-2}) and ultrathin (~ 11.5 nm) to reduce cost, offers homogenized electron/ion flux to enable low-barrier and uniform Mg deposition on the Cu foil surface (Figure 1e). The

compact structure of the Mg deposits is beneficial for reduced interfacial resistance, facile Mg^{2+} ion transport, and inhibited parasitic reactions during Mg plating/stripping processes. Consequently, the Mg-plated Au-Cu electrode demonstrates outstanding CE and prolonged cycle lifespan with high Mg metal utilization of 75%, as compared to the bare Cu electrode counterpart. The full cell assembled with a Mg-plated Au-Cu anode and a Mo_6S_8 cathode achieves remarkable electrochemical properties in terms of cycling stability, capacity retention, and capacity utilization at a low negative/positive (N/P) ratio.

RESULTS AND DISCUSSION

The growth of a conformal Au coating on the surface of commercial Cu foils was conducted using an ion beam sputtering method. Figure 2a and S1 shows the wide-angle X-ray scattering (WAXS) results of Cu foil before and after the 150s sputtering, where the peak located at 38.1° can be ascribed to the (111) lattice plane of metallic Au (PDF # 04-0784). From the scanning electron microscopy (SEM) and atomic force microscopy (AFM) observations, the obtained Au-Cu foil exhibits a relatively smooth surface with dense and evenly anchored Au nanoparticles, contrasting the rough surface of bare Cu foil (Figure 2b, c and Figure S2 and S3). A distinct change in color between bare Cu and Au-Cu foils can also be observed from their digital photos in Figure 2b and c. The energy dispersive spectroscopy (EDS) images (Figure S4) further verify a uniform and complete coverage of Au coating on the Cu foil surface. It is worth emphasizing that the Au coating has a mass loading of ~ 0.11 mg cm^{-2} and a thickness

of ~ 11.5 nm from the focused ion beam (FIB)-SEM observation in Figure S5, accounting for only 1.1 wt% of 9 μm Cu foil, which is essential for avoiding high cost and significant reduction of cell energy density. Furthermore, the Au-Cu foil can be fabricated on a large scale to meet the requirement of practical applications (Figure S6). With the successful synthesis of Au-coated Cu foil, we first compared the magnesiophilicity of Au and Cu surfaces by density functional theory (DFT) calculations. The binding energy (E_b) of the Au (111) surface toward a Mg atom is -0.83 eV, much larger than the value of -0.21 eV obtained on the Cu (111) surface (Figure 2d), suggesting that the Au coating has a better Mg affinity than the Cu substrate. Notably, the interaction between Mg and Au is also stronger than that between Mg and three 1,2-dimethoxyethane (DME) molecules (-0.74 eV, Figure S7), a typical solvated $[Mg(DME)_3]^{2+}$ ion pair in conventional ether electrolyte.[11, 15] From these theoretical results, the magnesiophilicity of Cu foil is seen to be enhanced by the Au coating, which is conducive to regulating the magnesium desolvation/transfer kinetics and deposition behavior.

To verify this conjecture, bare Cu and Au-Cu foils were employed as working electrodes to pair with Mg counter electrodes in an asymmetric cell configuration. 0.3 M magnesium triflate ($Mg(OTf)_2$) and 0.2 M magnesium chloride ($MgCl_2$) in DME was chosen as the electrolyte due to its cost-effectiveness and high stability for RMBs.[39] During the first magnesium plating on the bare Cu and Au-Cu electrodes (Figure S8), the voltage curves experience a sharp voltage spike (caused by Mg nucleation) and then reach a plateau state (related to continuous Mg growth). Generally, the difference

between the peak value of the voltage spike where nucleation initiates and the voltage value of the subsequent stable platform is defined as nucleation overpotential (μ_n), whereas the voltage difference between the plating platform and the zero-baseline is defined as plateau overpotential (μ_p).[40] Compared with the bare Cu electrode, which gives high μ_n and μ_p values of 1.71 and 0.35 V, the Au-Cu electrode possesses much smaller values of 1.35 and 0.29 V, respectively. From the electrochemical impedance spectroscopy (EIS) plots (Figure S9), charge transfer resistance (R_{ct}) is seen to experience sharp reduction by replacing bare Cu (119.0 kΩ) with Au-Cu electrodes (87.7 kΩ). The low deposition overpotentials and small interfacial impedance show that the highly magnesiophilic Au coating facilitates fast Mg transport at the electrolyte/electrode interface and subsequent deposition on the electrode surface.[41-43]

The scanning electron microscopy (SEM) images of the Cu and Au-Cu electrodes during the magnesium plating processes were collected in Figure 2e, f and Figure S10 and S11. Under a plating capacity of 0.5 mAh cm^{-2}, the bare Cu electrode surface is scattered by micron-sized Mg lumps (Figure S10a). These lumpy Mg deposits merge into large aggregates with cracks on the surface and in the cross-section of the deposition layer when the plating capacity is further increased to 2 mAh cm^{-2} (Figure 2e and Figure S11a). Interestingly, when the Au-Cu electrode is used, the plated Mg becomes continuous at the early stage (Figure S10b) and further grows into a uniform and compact Mg layer devoid of cracks (Figure 2f and Figure S11b). The thickness of the Mg deposition layer on the Au-Cu electrode is approximately 5 μm (inset of Figure 2f), close to the theoretical value with an Mg plating capacity of 2 mAh cm^{-2}. These

SEM observations strongly support the effectiveness of the Au coating in guiding homogeneous Mg deposition.

The Mg deposition behavior depends heavily upon the ion flux distribution at the electrode/electrolyte interface. The modulation effect of Au coating on the interfacial Mg-ion concentration field was simulated and visualized by finite element analysis methods with COMSOL Multiphysics software.[44, 45] Based on the SEM observation, protuberances (~ 0.2 μm) and Au nanoparticles (~ 50 nm) are introduced on the surface of bare Cu and Au-Cu electrodes in the designed models, respectively (Figure S12). For the bare Cu electrode (Figure 2g), the Mg^{2+} ion flux around the protrusions is found to be higher than that in other regions, which strengthens the surrounding electric field intensity, consequently leading to inhomogeneous magnesium deposition. Encouragingly, the Au-Cu electrode possesses a very uniform distribution of Mg^{2+} ion flux across its whole surface (Figure 2h). These simulations, consistent with the SEM observation, further indicate the Au coating aids in homogenizing the Mg^{2+} flux distribution and guiding uniform magnesium deposition.

The beneficial effects of the Au coating on Mg nucleation and deposition behavior inspire us to probe the cyclability of the Au-Cu electrode in the Mg||Cu cells. The asymmetric cells with bare Cu and Au-Cu electrodes were first cycled at a current density of 1 mA cm^{-2} with a fixed plating capacity of 1 mAh cm^{-2} and a cutoff voltage of 1 V for stripping. The CE can be calculated from the ratio of stripped capacity to the plated capacity during the same cycle.[46] For the cell with a bare Cu electrode (Figure 3a and S13), sharp fluctuations in the efficiency curves are observed, in which the CE

cannot reach 99.12% until the 25th cycle and decreases to almost zero after 380 cycles. On the contrary, the initial CE of the Au-Cu electrode reaches 89.42%, and the CE increases to 99.88% in the 2nd cycle and holds steadily in the following 500 plating/stripping cycles. The superiority of the magnesiophilic Au coating is further validated at 3 mA cm^{-2} and 3 mAh cm^{-2}. As shown in Figure S14, the bare Cu electrode only sustains 179 cycles prior to a short circuit, while the Au-Cu electrode exhibits greatly improved cycling stability with a low charge-discharge voltage gap over 300 cycles. The enhanced performance of Au-Cu electrode should be attributed to the magnesiophilic and highly conductive properties of Au coating, which is beneficial for lowering the nucleation overpotential (Figure S8 and S14), guiding uniform deposition of magnesium (Figure S15), and boosting ionic transport (Figure S9) during the long-term plating/stripping.

To meet practical battery requirements, the CE of the Mg||Cu cells was further examined under the high depth of discharge (DOD) conditions. First, a Mg plating/stripping cycle was preconditioned to stabilize and activate the asymmetric cell.[13, 47] Next, a Mg reservoir (Q_T) was plated onto Au-Cu foil to form a Mg-plated Au-Cu electrode. The composite Mg electrode with capacity Q_T was then cycled with a fixed capacity (Q_C) for n cycles and finally stripped to 1 V (Q_S). The average CE can be calculated by dividing the total stripped capacity ($nQ_C + Q_S$) by the total plated capacity ($nQ_C + Q_T$). The DOD (or capacity utilization) of the Mg-plated Au-Cu electrode is given by Q_C/Q_T. As displayed in Figure 3b, at 50% DOD (Q_T =1 mAh cm^{-2} and Q_C =0.5 mAh cm^{-2}) with a current density of 0.5 mA cm^{-2}, the charge potential of

the bare Cu electrode quickly increases to the cutoff limit of 1.0 V after 50 h, giving an average CE of 92.59%, which is very different what is observed in Figure 3a. This phenomenon is most likely caused by the quick exhaustion of limited active Mg subjected to the magnesiophobic and inhomogeneous Mg plating/stripping behavior of the bare Cu foil. Upon introducing the magnesiophilic Au coating, the cycling life and average CE of the Au-Cu electrodes are greatly improved to 300 h and 98.67% respectively, with a much slower increase in overpotential under the same testing conditions (Figure 3c). As for different Au sputtering times (from 50 to 200 s), the Au-Cu electrode formed by 150 s sputtering was found to be optimal (Figure S16), hence it was used for further characterization.

When the Q_T and Q_C were increased to 5 and 2.5 mAh cm^{-2} respectively (Figure 3d), the average CE of the Au-Cu electrode was 99.43% after 10 cycles at 50% DOD. Upon further increasing the DOD to 75% (Q_T =5 mAh cm^{-2} and Q_C =3.75 mAh cm^{-2}), the Au-Cu electrode can still exhibit an average CE of 99.16% after 10 cycles at 0.5 mA cm^{-2}. Notably, the volumetric capacity of the composite magnesium anode reaches 2874 mAh cm^{-3} under a 75% DOD_{Mg} cycling condition, which far exceeds the theoretical specific capacity of metallic Li (2046 mAh cm^{-3}) and graphite (818 mAh cm^{-3}). Compared with recent works on electrolyte engineering and current collector modification for Mg||Cu cells, our work has achieved one of the best performances in the literature in terms of highest Mg utilization (Figure 3e and details in Table S1).

The surface chemistry of the Au-Cu electrode after 10 cycles was characterized by SEM, XRD, X-ray photoelectron spectroscopy (XPS), and time-of-flight secondary ion

mass spectrometry (TOF-SIMS). As presented in Figure 4a, b, and Figure S17, many residual "dead Mg" particles with nonuniform size and height appear on the surface of the bare cycled Cu electrode. In contrast, the cycled Au-Cu electrode exhibits a textured surface without noticeable residual Mg particles (Figure 4c, d, and Figure S18). Figure 4e, f, and S19 display the 3D views of TOF-SIMS signals of MgO_2^-, $MgCl^-$, MgF^-, MgS^-, $C_2H_3O^-$, and $CF_3SO_3^-$ fragments, which are the main decomposition products of $Mg(OTf)_2$, $MgCl_2$, and DME in the electrolyte.[48, 49] All these signals detected on the Au-Cu electrode after cycling exhibit reduced thickness and enhanced homogeneity compared with those observed on the bare cycled Cu electrode. The high-resolution C *1s*, Mg *2p*, and O *1s* XPS spectra (Figure 4g and Figure S20) demonstrate weaker $MgCO_3$ signals on the surface of cycled Au-Cu electrode when compared with that of cycled Cu electrode.[50, 51] As a typical resistive component,[29] $MgCO_3$ affords a high Mg diffusion barrier (2.17 eV, Figure S21). Furthermore, Au *4f* signals observed from the XPS spectra (Figure 4h) and X-ray diffraction (XRD) patterns (Figure S22) exhibit minor changes before and after cycling,[52] indicating that the Au coating layer is (electro)chemically stable and can be anchored tightly onto the Cu substrate. It is demonstrated that Au with a low diffusion barrier ($\sim$ 0.033 eV) can help to inhibit uneven Mg deposition.[38] These results indicate that the decomposition of the ether electrolyte during cycling is suppressed on the surface of the Mg-plated Au-Cu electrode, which is attributed to its compact and uniform surface that can effectively reduce the accessible surface area to liquid electrolyte.

As a proof of concept, we employed the Au-Cu electrode to fabricate full cells. Chevrel phase Mo_6S_8 is selected as the cathode for its proven excellent cycling stability in ether electrolytes.[11, 53] The Mg-plated Au-Cu composite electrode with limited Mg was used as the anode (Mg@Au-Cu). The Mo_6S_8||Mg@Cu batteries were also assembled for comparison. Figure 5a compares the initial discharge-charge curves at a current density of 50 mA g^{-1}, where the discharge capacities of the full cells with Mg@Cu and Mg@Au-Cu anodes are similar (83.1 *vs.* 84.7 mAh g^{-1}). However, Mo_6S_8||Mg@Au-Cu cell reaches a higher CE of 64.78% than that of the control cell (50.40%), indicating that more magnesium intercalated into the cathode can be stripped and deposited back onto the Cu electrode with the assistance of magnesiophilic Au coating. Moreover, the polarization voltages (ΔE), defined as the voltage difference at 50% of the charge and discharge capacities, are 0.90 V and 1.59 V for Mo_6S_8||Mg@Au-Cu and Mo_6S_8||Mg@Cu cells, respectively. The lower ΔE, consistent with the smaller R_{ct} observed from the EIS spectra (Figure S23), indicates faster Mg^{2+} ion diffusion kinetics on the Au-Cu electrode during the charge-discharge processes. The cycling performances of full cells with a low N/P ratio of 1.33 are examined at 100 mA g^{-1} as shown in Figure 5b and c. In contrast to the Mo_6S_8||Mg@Cu cell experiencing sharp capacity decay within 20 cycles, the Mo_6S_8||Mg@Au-Cu cell yields a reversible capacity of 32.3 mAh g^{-1} after 300 cycles with a capacity retention of 80% and an average CE of 99.10%. The capacity increase in the initial cycles is associated with the activation of the Mg^{2+} intercalation process in Mo_6S_8.[24] With the rise of N/P ratios (Figure S24-26), the capacities of the Mo_6S_8||Mg@Au-Cu full cells are increased, and

the activation process becomes shorter, whereas the control cell with bare Cu electrode still shows negligible capacity. These results further confirm the practicability of the Au-Cu electrode as a current collector of composite Mg anode for high-performance RMBs.

CONCLUSION

In summary, we developed a deeply cyclable and highly reversible composite Mg metal anode using a magnesiophilic Au coating-modified commercial Cu foil. The experimental investigation, DFT calculation, and COMSOL simulation reveal that the magnesiophilic Au coating can facilitate fast Mg-ion transport, homogenize electric field and ionic flux distribution, decrease Mg nucleation overpotential, guide uniform Mg deposition, and protect Mg metal from parasitic reactions. Consequently, the Mg-plated Au-Cu electrode delivers a high average CE of 99.16% for over 170 h cycling with a high Mg metal utilization (75%). This work sheds light on the rational design of composite Mg anodes with high utilization and reversibility, spurring the development of future high-energy-density RMBs.

ASSOCIATED CONTENT

Supporting Information.

The Supporting Information is available free of charge at

Experimental details, SEM images, AFM images, EDS mappings, digital photos, EIS spectra, XRD patterns, XPS spectra, and galvanostatic charge-discharge profiles.

AUTHOR INFORMATION

Notes

The authors declare no competing financial interest.

Acknowledgments

Z. W. S. acknowledges the Singapore National Research Foundation (NRF-NRFF2017-04) and Agency for Science, Technology and Research (Central Research Fund Award). Z. S. acknowledges the Czech Science Foundation (GACR no. 20-16124J). M.-F. N. acknowledges the National Supercomputing center (NSCC) Singapore and A*STAR Computational Resource center (A*CRC) of Singapore through the use of its high performance computing facilities. The authors thank Debbie Seng Hwee Leng for technical assistance in operating XPS, Zhenxiang Xing for assistance in TOF-SIMS analysis, and Siew Lang Teo assistance in FIB-SEM analysis.

REFERENCES

(1) Sun, Y.; Liu, N.; Cui, Y. Promises and challenges of nanomaterials for lithium-based rechargeable batteries. *Nat. Energy* **2016,** *1*, 16071.

(2) Liang, Y.; Dong, H.; Aurbach, D.; Yao, Y. Current status and future directions of multivalent metal-ion batteries. *Nat. Energy* **2020**, *5*, 1646-656.

(3) Zhang, W.; Zhao, Q.; Hou, Y.; Shen, Z.; Fan, L.; Zhou, S.; Lu, Y.; Archer, L. A. Dynamic Interphase-Mediated Assembly for Deep Cycling Metal Batteries. *Sci. Adv.* **2021**, *7*, 3752.

(4) Li, Y.; Wang, C.; Wang, W.; Eng, A. Y. S.; Wan, M. Fu, L.; Mao, E.; Li, G.; Tang, J.; Seh, Z. W.; Sun, Y. Enhanced Chemical Immobilization and Catalytic Conversion of Polysulfide Intermediates Using Metallic Mo Nanoclusters for

High-Performance Li-S Batteries. *ACS Nano* **2020**, *14*, 1148-1157.

(5) Hou, S.; Ji, X.; Gaskell, K.; Wang, P.-F.; Wang, L.; Xu, J.; Sun, R.; Borodin, O.; Wang, C. Solvation sheath reorganization enables divalent metal batteries with fast interfacial charge transfer kinetics. *Science* **2021**, *374*, 172-178.

(6) Aurbach, D.; Lu, Z.; Schechter, A.; Gofer, Y.; Gizbar, H.; Turgeman, R.; Cohen, Y.; Moshkovich, M.; Levi, E. Prototype systems for rechargeable magnesium batteries. *Nature* **2000**, *407*, 724-727.

(7) Bae, J.; Park, H.; Guo, X.; Zhang, X.; Warner, J. H.; Yu, G. High-performance magnesium metal batteries via switching the passivation film into a solid electrolyte interphase. *Energy Environ. Sci.* **2021,** *14*, 4391-4399.

(8) Dong, H.; Liang, Y.; Tutusaus, O.; Mohtadi, R.; Zhang, Y.; Hao, F.; Yao, Y. Directing Mg-Storage Chemistry in Organic Polymers toward High-Energy Mg Batteries. *Joule* **2019**, *3*, 782-793.

(9) Attias, R.; Salama, M.; Hirsch, B.; Goffer, Y.; Aurbach, D. Anode-Electrolyte Interfaces in Secondary Magnesium Batteries. *Joule* **2019**, *3*, 27-52.

(10) Liang, Z.; Ban, C. Strategies to Enable Reversible Magnesium Electrochemistry: From Electrolytes to Artificial Solid-Electrolyte Interphases. *Angew. Chem.* **2021,** *60*, 11036-11047.

(11) Sun, Y.; Ai, F.; Lu, Y. C. Electrolyte and Interphase Design for Magnesium Anode: Major Challenges and Perspectives. *Small* **2022**, *18*, 2200009.

(12) Ren, W.; Wu, D.; NuLi, Y.; Zhang, D.; Yang, Y.; Wang, Y.; Yang, J.; Wang, J. An Efficient Bulky $Mg[B(Otfe)_4]_2$ Electrolyte and Its Derivatively General Design Strategy for Rechargeable Magnesium Batteries. *ACS Energy Lett.* **2021**, *6*, 3212-3220.

(13) Dong, H.; Tutusaus, O.; Liang, Y.; Zhang, Y.; Lebens-Higgins, Z.; Yang, W.; Mohtadi, R.; Yao, Y. High-power Mg batteries enabled by heterogeneous enolization redox chemistry and weakly coordinating electrolytes. *Nat. Energy* **2020**, *5,* 1646-656.

(14) Xiao, J.; Zhang, X.; Fan, H.; Zhao, Y.; Su, Y.; Liu, H.; Li, X.; Su, Y.; Yuan, H.; Pan, T.; Lin, Q.; Pan, L.; Zhang, Y. Stable Solid Electrolyte Interphase In Situ Formed

on Magnesium-Metal Anode by using a Perfluorinated Alkoxide-Based All-Magnesium Salt Electrolyte. *Adv. Mater.* **2022**, *34*, 2203783.

(15) Zhao, W.; Pan, Z.; Zhang, Y.; Liu, Y.; Dou, H.; Shi, Y.; Zuo, Z.; Zhang, B.; Chen, J.; Zhao, X.; Yang, X. Tailoring Coordination in Conventional Ether-Based Electrolytes for Reversible Magnesium-Metal Anodes. *Angew. Chem.* **2022**, *134*, e202205187.

(16) Sun, Y.; Zou, Q.; Wang, W.; Lu, Y.-C. Non-passivating Anion Adsorption Enables Reversible Magnesium Redox in Simple Non-nucleophilic Electrolytes. *ACS Energy Lett.* **2021**, *6*, 3607-3613.

(17) Park, H.; Lim, H.-K.; Oh, S. H.; Park, J.; Lim, H.-D.; Kang, K. Tailoring Ion-Conducting Interphases on Magnesium Metals for High-Efficiency Rechargeable Magnesium Metal Batteries. *ACS Energy Lett.* **2020,** *5*, 3733-3740.

(18) Li, Z.; Diemant, T.; Meng, Z.; Xiu, Y.; Reupert, A.; Wang, L.; Fichtner, M.; Zhao-Karger, Z. Establishing a Stable Anode-Electrolyte Interface in Mg Batteries by Electrolyte Additive. *ACS Appl. Mater. Interfaces* **2021,** *13*, 33123-33132.

(19) Lv, R.; Guan, X.; Zhang, J.; Xia, Y.; Luo, J. Enabling Mg metal anodes rechargeable in conventional electrolytes by fast ionic transport interphase. *Nat. Sci. Rev.* **2020,** *7*, 333-341.

(20) Son, S. B.; Gao, T.; Harvey, S. P.; Steirer, K. X.; Stokes, A.; Norman, A.; Wang, C.; Cresce, A.; Xu, K.; Ban, C. An artificial interphase enables reversible magnesium chemistry in carbonate electrolytes. *Nat. Chem.* **2018,** *10*, 532-539.

(21) Zhao, Y.; Du, A.; Dong, S.; Jiang, F.; Guo, Z.; Ge, X.; Qu, X.; Zhou, X.; Cui, G. A Bismuth-Based Protective Layer for Magnesium Metal Anode in Noncorrosive Electrolytes. *ACS Energy Lett.* **2021**, *6*, 2594-2601.

(22) Wei, C.; Tan, L.; Zhang, Y.; Xi, B.; Xiong, S.; Feng, J.; Qian, Y. Highly reversible Mg metal anodes enabled by interfacial liquid metal engineering for high-energy Mg-S batteries. *Energy Storage Mater.* **2022,** *48*, 447-457.

(23) Tang, K.; Du, A.; Du, X.; Dong, S.; Lu, C.; Cui, Z.; Li, L.; Ding, G.; Chen, F.; Zhou, X.; Cui, G. A Novel Regulation Strategy of Solid Electrolyte Interphase Based on Anion-Solvent Coordination for Magnesium Metal Anode. *Small* **2020**, *16*,

2005424.

(24) Du, A.; Zhang, Z.; Qu, H.; Cui, Z.; Qiao, L.; Wang, L.; Chai, J.; Lu, T.; Dong, S.; Dong, T.; Xu, H.; Zhou, X.; Cui, G. An Efficient Organic Magnesium Borate-based Electrolyte with Non-Nucleophilic Characteristics for Magnesium-Sulfur Battery. *Energy Environ. Sci.* **2017,** *10*, 2616-2625.

(25) Yang, Y.; Qiu, Y.; NuLi, Y.; Wang, W.; Yang, J.; Wang, J. A Novel Magnesium Electrolyte Containing a Magnesium Bis(diisopropyl)amide-Magnesium Chloride Complex for Rechargeable Magnesium Batteries. *J. Mater. Chem. A* **2019,** *7*, 18295-18303.

(26) Wang, F.; Wu, D.; Zhuang, Y.; Li, J.; Nie, X.; Zeng, J.; Zhao, J. Modification of a Cu Mesh with Nanowires and Magnesiophilic Ag Sites to Induce Uniform Magnesium Deposition. *ACS Appl. Mater. Interfaces* **2022**, *14*, 31148–31159

(27) Lim, H. D.; Kim, D. H.; Park, S.; Lee, M. E.; Jin, H. J.; Yu, S.; Oh, S. H.; Yun, Y. S. Magnesiophilic Graphitic Carbon Nanosubstrate for Highly Efficient and Fast-Rechargeable Mg Metal Batteries. *ACS Appl. Mater. Interfaces* **2019,** *11*, 38754-38761.

(28) Song, Z.; Zhang, Z.; Du, A.; Dong, S.; Li, G.; Cui, G. Uniform Magnesium Electrodeposition via Synergistic Coupling of Current Homogenization, Geometric Confinement, and Chemisorption Effect. *Adv. Mater.* **2021,** *33*, 2100224.

(29) Lin, L.; Suo, L.; Hu, Y. s.; Li, H.; Huang, X.; Chen, L. Epitaxial Induced Plating Current‐Collector Lasting Lifespan of Anode‐Free Lithium Metal Battery. *Adv. Energy Mater.* **2021**, *11*, 2003709

(30) Du, J.; Wang, W.; Wan, M.; Wang, X.; Li, G.; Tan, Y.; Li, C.; Tu, S.; Sun, Y. Doctor‐Blade Casting Fabrication of Ultrathin Li Metal Electrode for High‐Energy‐Density Batteries. *Adv. Energy Mater.* **2021**, *11,* 2102259.

(31) Wang, X.; He, Y.; Tu, S.; Fu, L.; Chen, Z.; Liu, S.; Cai, Z.; Wang, L.; He, X.; Sun, Y. Li plating on alloy with superior electro-mechanical stability for high energy density anode-free batteries. *Energy Storage Mater.* **2022,** *49*, 135-143.

(32) Davidson, R.; Verma, A.; Santos, D.; Hao, F.; Fincher, C.; Xiang, S.; Van Buskirk, J.; Xie, K.; Pharr, M.; Mukherjee, P. P.; Banerjee, S. Formation of Magnesium

Dendrites during Electrodeposition. *ACS Energy Lett.* **2018,** *4*, 375-376.

(33) Davidson, R.; Verma, A.; Santos, D.; Hao, F.; Fincher, C. D.; Zhao, D.; Attari, V.; Schofield, P.; Van Buskirk, J.; Fraticelli-Cartagena, A.; Alivio, T. E. G.; Arroyave, R.; Xie, K.; Pharr, M.; Mukherjee, P. P.; Banerjee, S. *Mater. Horizons* **2020,** *7*, 843-854.

(34) Song, Z.; Zhang, Z.; Du, A.; Dong, S.; Li, G.; Cui, G. Insights into interfacial speciation and deposition morphology evolution at Mg-electrolyte interfaces under practical conditions. *J. Energy Chem.* **2020**, *48*, 299-307.

(35) Janna Eaves-Rathert, K. M., Murtaza Zohair, and Cary L. Kinetic- versus Diffusion-Driven Three Dimensional Growth in Magnesium Metal Battery Anodes, Pint. *Joule* **2020**, *4*, 1324-1336.

(36) Li, Y.; Zhou, X.; Hu, J.; Zheng, Y.; Huang, M.; Guo, K.; Li, C. Reversible Mg metal anode in conventional electrolyte enabled by durable heterogeneous SEI with low surface diffusion barrier. *Energy Storage Mater.* **2022,** *46*, 1-9.

(37) Huang, D.; Tan, S.; Li, M.; Wang, D.; Han, C.; An, Q.; Mai, L. Highly Efficient Non-Nucleophilic $Mg(CF_3SO_3)_2$-Based Electrolyte for High-Power Mg/S Battery. *ACS Appl. Mater. Interfaces* **2020,** *12*, 17474-17480.

(38) Kwak, J. H.; Jeoun, Y.; Oh, S. H.; Yu, S.; Lim, J.-H.; Sung, Y.-E.; Yu, S.-H.; Lim, H.-D. Operando Visualization of Morphological Evolution in Mg Metal Anode: Insight into Dendrite Suppression for Stable Mg Metal Batteries. *ACS Energy Lett.* **2021**, *6*, 162-170.

(39) Nguyen, D.-T.; Eng, A. Y. S.; Ng, M.-F.; Kumar, V.; Sofer, Z.; Handoko, A. D.; Subramanian, G. S.; Seh, Z. W. A High-Performance Magnesium Triflate-based Electrolyte for Rechargeable Magnesium Batteries. *Cell Rep. Phy. Sci.* **2020**, *1*, 100265.

(40) Lee, S.; Woo Kang, D.; Hwan Kwak, J.; Shin, S.; Park, J.-W.; Yu, S.-H.; Jung, H.-G.; Gon Kim, B.; Lim, H.-D. Gold-Incorporated Porous Hollow Carbon Nanofiber for Reversible Magnesium-Metal Batteries. *Chem. Engin. J.* **2022,** *431*, 133968.

(41) Chen, Y.; Xu, X.; Gao, L.; Yu, G.; Kapitanova, O. O.; Xiong, S.; Volkov, V. S.; Song, Z.; Liu, Y. Two Birds with One Stone: Using Indium Oxide Surficial

Modification to Tune Inner Helmholtz Plane and Regulate Nucleation for Dendrite-free Lithium Anode. *Small Methods* **2022**, *6*, 2200113.

(42) Wang, J.; Luo, N.; Wu, J.; Huang, S.; Yu, L.; Wei, M, Hierarchical spheres constructed by ultrathin VS_2 nanosheets for sodium-ion batteries. *J. Mater. Chem. A*, **2019**, *7*, 3691-3696.

(43) Xu, D.; Chao, D.; Wang, H.; Gong, Y.; Wang, R.; He, B.; Hu, X.; Fan, H. J. Flexible Quasi-Solid-State Sodium-Ion Capacitors Developed Using 2D Metal-Organic-Framework Array as Reactor. *Adv. Energy. Mater.* **2018**, *8*, 1702769.

(44) Hu, A.; Chen, W.; Du, X.; Hu, Y.; Lei, T.; Wang, H.; Xue, L.; Li, Y.; Sun, H.; Yan, Y.; Long, J.; Shu, C.; Zhu, J.; Li, B.; Wang, X.; Xiong, J. An artificial hybrid interphase for an ultrahigh-rate and practical lithium metal anode. *Energy Environ. Sci.* **2021**, *14*, 4115-4124.

(45) Liao, Y.; Yuan, L.; Liu, X.; Meng, J.; Zhang, W.; Li, Z.; Huang, Y. Low-cost fumed silicon dioxide uniform Li^+ flux for lean-electrolyte and anode-free Li/S battery. *Energy Storage Mater.* **2022,** *48*, 366-374.

(46) Liu, Y.; Wu, X.; Niu, C.; Xu, W.; Cao, X.; Zhang, J.-G.; Jiang, X.; Xiao, J.; Yang, J.; Whittingham, M. S.; Liu, J. Systematic Evaluation of Carbon Hosts for High-Energy Rechargeable Lithium-Metal Batteries. *ACS Energy Lett.* **2021**, *6*, 1550-1559.

(47) Adams, B. D.; Zheng, J.; Ren, X.; Xu, W.; Zhang, J.-G. Accurate Determination of Coulombic Efficiency for Lithium Metal Anodes and Lithium Metal Batteries. *Adv. Energy Mater.* **2018**, *8*, 1702097.

(48) Dou, H.; Zhao, X.; Zhang, Y.; Zhao, W.; Yan, Y.; Ma, Z.-F.; Wang, X.; Yang, X. Revisiting the Degradation of Solid/Electrolyte Interfaces of Magnesium Metal Anodes: Decisive Role of Interfacial Composition. *Nano Energy* **2021,** *86*, 106087.

(49) Zhang, Y.; Li, J.; Zhao, W.; Dou, H.; Zhao, X.; Liu, Y.; Zhang, B.; Yang, X. Defect-Free Metal-Organic Framework Membrane for Precise Ion/Solvent Separation toward Highly Stable Magnesium Metal Anode. *Adv. Mater.* **2021**, *33*, 2108114.

(50) Nguyen, D.-T.; Eng, A. Y. S.; Horia, R.; Sofer, Z.; Handoko, A. D.; Ng, M.-F.; Seh, Z. W. Rechargeable magnesium batteries enabled by conventional electrolytes with

multifunctional organic chloride additives. *Energy Storage Mater.* **2022,** *45*, 1120-1132.

(51) Horia, R.; Nguyen, D. T.; Eng, A. Y. S.; Seh, Z. W. Using a Chloride-Free Magnesium Battery Electrolyte to Form a Robust Anode-Electrolyte Nanointerface. *Nano Lett.* **2021**, *21*, 8220-8228.

(52) Xiang, J.; Yuan, L.; Shen, Y.; Cheng, Z.; Yuan, K.; Guo, Z.; Zhang, Y.; Chen, X.; Huang, Y. Improved Rechargeability of Lithium Metal Anode via Controlling Lithium-Ion Flux. *Adv. Energy Mater.* **2018**, *8*, 1802352.

(53) Mao, M.; Lin, Z.; Tong, Y.; Yue, J.; Zhao, C.; Lu, J.; Zhang, Q.; Gu, L.; Suo, L.; Hu, Y. S.; Li, H.; Huang, X.; Chen, L. Iodine Vapor Transport-Triggered Preferential Growth of Chevrel Mo_6S_8 Nanosheets for Advanced Multivalent Batteries. *ACS Nano* **2020**, *14*, 1102-1110.

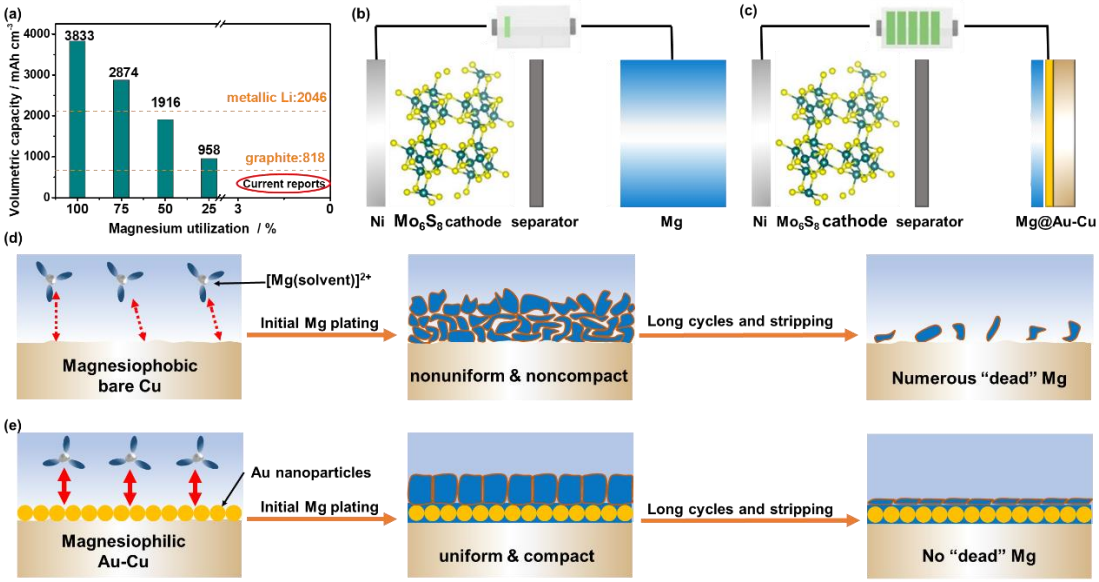

Figure 1. Schematic design concepts of the magnesiophilic Au coating modified Cu electrode to enable deeply cycled and highly reversible composite Mg metal anodes for high-energy-density RMBs. (a) The volumetric capacity of Mg anode with different utilizations. Schematic illustration of Mg metal full cells with (b) a Mg foil anode with ample excess capacity, showing poor energy density, and (c) a Mg-plated Au-Cu composite anode with high capacity utilization, achieving high energy density. Schematic illustration of Mg plating/stripping behavior on (d) bare Cu and (e) Au-Cu electrodes, showing that the magnesiophilic Au coating can homogenize electric field and ionic flux distribution, guide uniform Mg deposition, and suppress "dead" Mg formation on Cu electrode surface.

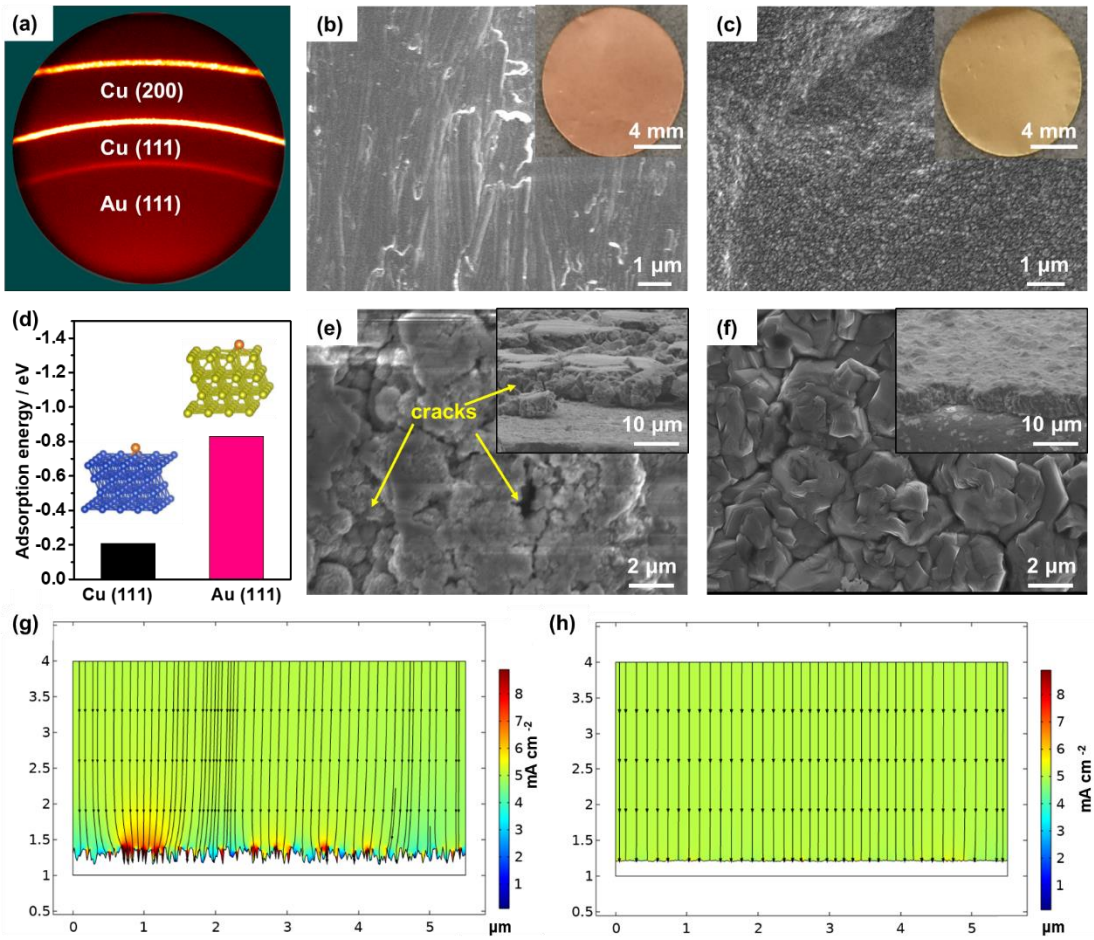

Figure 2. Characterization of the Au-Cu electrode. (a) WAXS results of Au-Cu foils. (b, c) SEM images and digital photos of (b) bare Cu and (c) Au-Cu foils. (d) Adsorption configuration and corresponding binding energy of Mg adsorbed on Cu (111) and Au (111) facets. Here, the blue, yellow, and dark yellow balls represent Cu, Au, and Mg, atoms respectively. SEM images of Mg plating on (e) bare Cu and (f) Au-Cu foils with a capacity of 2 mAh cm^{-2}. Simulation of the distributions of local current density on the (g) bare Cu and (h) Au-Cu electrodes at 5 mA cm^{-2}. Here, the color corresponds to local current density, black lines represent ion-flux streamlines.

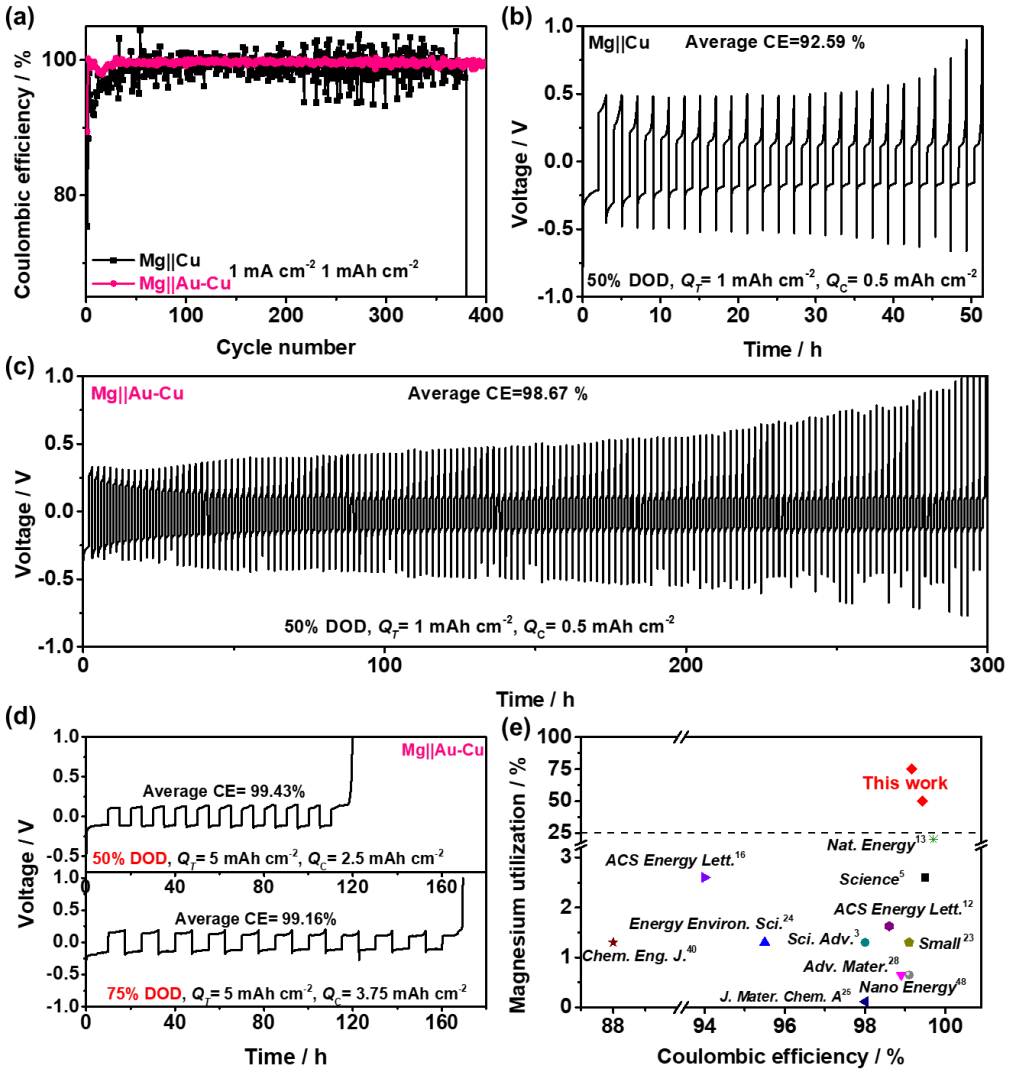

Figure 3. The electrochemical performance of the Au-Cu electrode in Mg||Au-Cu asymmetric cells. (a) Cycling performances of Mg||Cu and Mg||Au-Cu asymmetric cells with a capacity of 1 mAh cm^{-2} under 1 mA cm^{-2}. (b, c) The long-term cycling performance of the Mg||Cu and Mg||Au-Cu asymmetric cells at 50% DOD (Q_C =0.5 mAh cm^{-2}) under 0.5 mA cm^{-2}. (d) The voltage versus time plots of Mg||Au-Cu asymmetric cells at 50% (Q_C =2.5 mAh cm^{-2}) and 75% (Q_C =3.25 mAh cm^{-2}) DOD under 0.5 mA cm^{-2}. (e) The comparison of CE at different degrees of magnesium utilization between our work and previous reports. The related data are collected from Table S1.

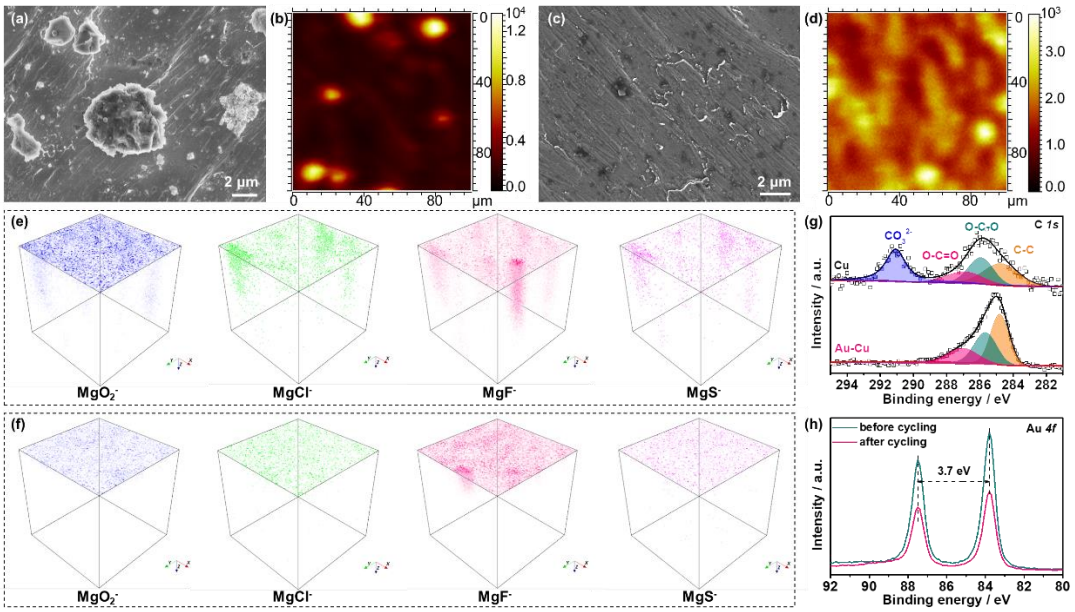

Figure 4. The surface chemistry of the Au-Cu electrode after 10 cycles in Mg||Au-Cu asymmetric cells. (a, c) SEM images, and (b, d) TOF-SIMS 2D render images of (a, b) bare Cu and (c, d) Au-Cu electrode surface after cycling. (e, f) 3D reconstruction of the sputtered volume of several secondary ion fragments of MgO_2^-, MgF^-, $MgCl^-$, and MgS^- of (e) bare Cu and (f) Au-Cu electrode surface after cycling. (g) C 1s XPS spectra of bare Cu and Au-Cu electrode surface after cycling. (h) Au 4f XPS spectra of Au-Cu electrode before and after cycling.

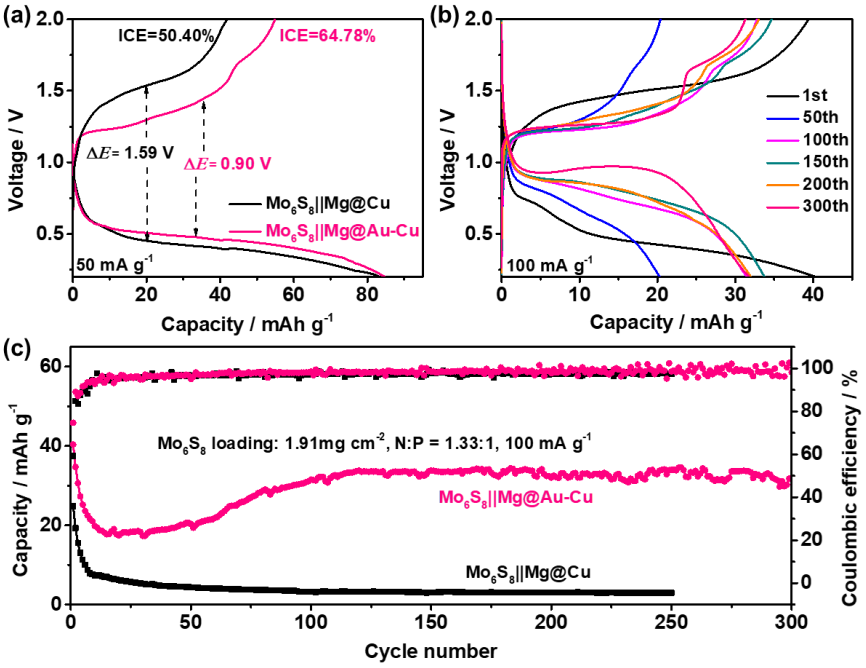

Figure 5. The electrochemical performance of the Au-Cu electrode in full cells. (a) The initial charge-discharge profiles of Mo_6S_8||Mg@Cu and Mo_6S_8||Mg@Au-Cu cells at 50 mA g^{-1}. (b) The long-term cycling performance and (c) corresponding charge-discharge profiles and of Mo_6S_8||Mg@Au-Cu cells at 100 mA g^{-1}.

Table of Content (TOC) Graphic